ELSEVIER

Physica D 152–153 (2001) 551–572

PHYSICA D

www.elsevier.com/locate/physd

Dispersive wave turbulence in one dimension

David Cai*, Andrew J. Majda, David W. McLaughlin, Esteban G. Tabak

Courant Institute of Mathematical Sciences, New York University, New York, NY 10012, USA

Abstract

In this article, we study numerically a one-dimensional model of dispersive wave turbulence. The article begins with a description of the model which we introduced earlier, followed by a concise summary of our previous results about it. In those previous studies, in addition to the spectra of weak turbulence (WT) theory, we also observed another distinct spectrum (the "MMT spectrum"). Our new results, presented here, include: (i) A detailed description of coexistence of spectra at distinct spatial scales, and the transitions between them at different temporal scales; (ii) The existence of a stable MMT front in k-space which separates the WT cascades from the dissipation range, for various forms of strong damping including "selective dissipation"; (iii) The existence of turbulent cycles in the one-dimensional model with focusing nonlinearity, induced by the interaction of spatially localized coherent structures with the resonant quartets of dispersive wave radiation; (iv) The detailed composition of these turbulent cycles — including the self-similar formation of focusing events (distinct in the forced and freely decaying cases), and the transport by the WT direct and inverse cascades of excitations between spatial scales. This one-dimensional model admits a very precise and detailed realization of these turbulent cycles and their components. Our numerical experiments demonstrate that a complete theory of dispersive wave turbulence will require a full description of the turbulent field over all spatial scales (including those of the forcing and dissipation), and over extremely long times (as the nonlinear turnover time becomes very long in the weakly nonlinear limit). And, in the focusing case, a complete theory must also incorporate the interaction of localized coherent structures with resonant radiation.

Keywords: Dispersive wave; Turbulence; One dimension; Weak turbulence theory

1. Introduction

Waves in nature, such as waves on the surface of the sea or waves in the atmosphere, are phenomena so complex that they must be described statistically. Such complex waves comprise stochastic states for which wave spectra (the average energy density as a function of the wavelength), rather than individual wave trajectories, are natural observables. In these stochastic states, the fundamental weakly nonlinear excitations consist in resonant wave–wave interactions, which are described statistically by the theories of dispersive wave turbulence. The goals of these theories include: (i) the prediction of wave spectra and other observable quantities; (ii) the parametrization of small scale behavior for large scale numerical simulations. Theories of dispersive wave turbulence play a role for nonlinear waves similar to that played by statistical physics for mechanics — namely, to provide macroscopic descriptions of observable phenomena. The validity and accuracy of these theories is difficult to assess, primarily because of

* Corresponding author. Fax: +1-212-995-4121.
E-mail address: cai@cims.nyu.edu (D. Cai).

0167-2789/01/$ – see front matter
PII: S0167-2789(01)00193-2

mathematical and computational difficulties in those nonlinear partial differential equations (PDEs) which provide the fundamental description of the waves' evolution.

Dispersive wave turbulence is a theory of the flow of wave excitations between spatial scales — fluxes in k-space [18,19]. It assumes that the turbulent state is one of "statistically steady flow in k-space". Excitations at one spatial scale (say a long spatial scale) are injected into the system by external forcing and are removed by dissipation which is restricted to a second spatial scale (say a short scale). At scales in-between, there is no forcing or damping, and the wave satisfies a conservative Hamiltonian system. Resonant wave–wave interactions transport the excitations, setting up a steady flow from the injection to the dissipation scales. At the intermediate scales (the "inertial" or "Kolmogorov" scales) the waves reside in a statistical state of steady flow in k-space, and their wave spectra should be universal. These wave spectra are described by two-point correlation functions $n(k, t)$,

$$n(k,t) \equiv \langle a(k,t)\bar{a}(k,t)\rangle\,,$$

where $a(k, t)$ denotes the spatial Fourier transform of the wave profile $q(x, t)$, and $\langle\,\rangle$ denotes an average — either an ensemble average, a local time average, or both. To characterize these two-point functions $n(k, t)$, closure approximations which rely upon weak nonlinearity and/or Gaussian random phase assumptions have been developed — approximations which are often ad hoc and difficult to validate.

In the inertial range, one can describe the waves by the complex amplitude a_k, satisfying the Hamiltonian system

$$\mathrm{i}\frac{\partial a_k}{\partial t} = \frac{\delta H}{\delta \bar{a}_k}, \tag{1}$$

if there is only one type of wave present in the nonlinear medium. We consider Hamiltonians of the form,

$$H = H_0 + H_{\mathrm{int}}, \tag{2}$$

where

$$H_0 = \int \omega(k) a_k \bar{a}_k \,\mathrm{d}k \tag{3}$$

is the Hamiltonian of the linearized problem, $\omega(k)$ denotes the dispersion relation, and H_{int} is a perturbation describing the interaction amongst those degrees of freedom represented, in k-space, by a_k. Generally, H_{int} can be expressed in terms of power series in a_k and $\bar{a}_k$, such as

$$\begin{aligned} H_{\mathrm{int}} = &\int (P_{kk_1k_2}\bar{a}_k a_{k_1} a_{k_2} + \bar{P}_{kk_1k_2} a_k \bar{a}_{k_1}\bar{a}_{k_2})\delta(k-k_1-k_2)\,\mathrm{d}k\,\mathrm{d}k_1\,\mathrm{d}k_2 \\ &+ \int (Q_{kk_1k_2} a_k a_{k_1} a_{k_2} + \bar{Q}_{kk_1k_2}\bar{a}_k\bar{a}_{k_1}\bar{a}_{k_2})\delta(k+k_1+k_2)\,\mathrm{d}k\,\mathrm{d}k_1\,\mathrm{d}k_2 \\ &+ \int R_{kk_1k_2k_3}\bar{a}_k\bar{a}_{k_1}a_{k_2}a_{k_3}\delta(k+k_1-k_2-k_3)\,\mathrm{d}k\,\mathrm{d}k_1\,\mathrm{d}k_2\,\mathrm{d}k_3 + \cdots . \end{aligned} \tag{4}$$

The dispersion relation $\omega(k)$ determines the nature of near linear wave–wave interactions. For example, if the following condition holds:

$$\omega(k) = \omega(k_1) + \omega(k_2), \quad k = k_1 + k_2 \tag{5}$$

for some k, the wave interaction leads to the resonant interaction of the waves a_{k_1} and a_{k_2} with $a_{k_1+k_2}$. This situation is called *three-wave* resonance. If (i) Eq. (5) does not have solutions, and if (ii) the following system has nontrivial ($k_3 \neq k_1, k_2$) solutions,

$$\omega(k_1) + \omega(k_2) = \omega(k_3) + \omega(k_4), \quad k_1 + k_2 = k_3 + k_4, \tag{6}$$

then the four-wave resonance is primarily responsible for the transfer of energy by weak dispersive waves. It can be easily shown that, under the above two conditions, a normal form near-identity transformation will place the Hamiltonian (2) in the form,

$$H = \int \omega(k) a_k \bar{a}_k \, \mathrm{d}k + \int S_{kk_1k_2k_3} \bar{a}_k \bar{a}_{k_1} a_{k_2} a_{k_3} \delta(k + k_1 - k_2 - k_3) \, \mathrm{d}k \, \mathrm{d}k_1 \, \mathrm{d}k_2 \, \mathrm{d}k_3, \tag{7}$$

where higher order nonlinearities have been neglected. This is the generic Hamiltonian system with four-wave resonances. Clearly, in this case, the "particle" number,

$$N = \int n_k \, \mathrm{d}k = \int n_\omega \, \mathrm{d}\omega, \tag{8}$$

where $n_k = |a_k|^2$ and $n_\omega = n_k \, \mathrm{d}k/\mathrm{d}\omega$, is conserved. In addition, the linear energy can be written as

$$H_0 = \int \omega_k n_k \, \mathrm{d}k = \int \omega n_\omega \, \mathrm{d}\omega. \tag{9}$$

This linear energy also plays an important role in the theory of weakly nonlinear dispersive wave turbulence.

In a dispersive wave turbulence whose dynamics is governed by Eq. (7), four-wave resonance is the dominant mechanism for transporting excitations between spatial scales, generating the *direct cascade* (toward short wavelengths) and the *inverse cascade* (toward long wavelengths). However, in nonlinear wave systems, localized coherent structures often coexist with resonant radiation. When both resonant radiation and coherent structures are present, theoretical descriptions of dispersive wave turbulence are even more difficult to construct. For example, the formation of coherent structures and their interaction with radiation may result in modifications of WT cascades, and must be incorporated into a theory of the mechanism for the energy transfer.

We [3,5,9] have been developing and studying a one-dimensional model system for dispersive wave turbulence in order to understand its properties and to clarify its theoretical representations. The single spatial dimension renders the waves nearly amenable to analytical description, and certainly to careful and controlled numerical simulation. Furthermore, our model system has tunable parameters which control dispersion and nonlinearity. This flexibility allows us not only to treat the model as a "toy system" for realistic physical waves, such as gravitational waves over deep waters, by choosing specific parameter values, but also to examine systematically the validity of WT theory by varying the parameter values over a wide range of parameter space.

After a very brief overview of standard weak turbulence (WT) theory, this article begins with a concise summary in Section 2.3 of our previous results [3,5,9] for a one-dimensional model of dispersive wave turbulence, introduced in [9]. In those previous studies, in addition to the spectra of WT theory, we also observed another distinct spectrum (which will be referred to as the "MMT spectrum"). Our new results, presented here, include the following.

In Section 3, we focus upon the temporal and spatial scales over which distinct spectra are observed. In particular, (i) we use the temporal growth of the L^2 norm to monitor a transition between the MMT and WT spectra. (ii) We show the existence of a stable MMT front in k-space which separates the WT cascades at intermediate spatial scales from the high k dissipation range, for various forms of strong damping, including "selective dissipation". This material in Section 3 emphasizes that (a) distinct wave spectra can coexist in distinct spatial scales, which (b) then compete over distinct time scales; moreover, (c) this competition is further complicated by very long nonlinear turnover times in precisely the weakly nonlinear limit for which WT is believed valid. These results of the interplay between the MMT and WT spectra show that a complete theory of dispersive wave turbulence will require a full description of the turbulent field across all spatial scales, including those of the forcing and dissipation.

In Section 4, we study (for our one-dimensional model with focusing nonlinearity) the interaction of spatially localized coherent structures with the resonant quartets of dispersive wave radiation. First, we describe two distinct self-similar focusing events — one for the free and another for the driven-damped case. These fast processes transfer

excitations from long spatial scales to shorter ones, and initiate turbulent cycles. These cycles are then studied in precise detail numerically, for different strengths of forcing and for the freely decaying case. The coexistence of the direct and inverse cascades within these cycles (as induced by the formation of localized structures), and the roles of both cascades in the transport of excitations between spatial scales, constitute the primary results of these numerical studies. We stress that this one-dimensional model admits a very precise and detailed realization of these turbulent cycles and their components. Finally, in Section 5, we summarize our results and mention an analogy with soap film turbulence.

2. Background summary

2.1. A one-dimensional model

In this paper, we study a class of one-dimensional nonlinear wave equations which was introduced in [9] as a simple model for which the validity of theories of dispersive wave turbulence could be precisely checked numerically. This model takes the form,

$$\mathrm{i}q_t = |\partial_x|^\alpha q \pm |\partial_x|^{-\sigma}(||\partial_x|^{-\sigma} q|^2 |\partial_x|^{-\sigma} q), \tag{10}$$

or equivalently in "k-space"

$$\mathrm{i}\dot{a}_k = \omega(k)a \pm \int \frac{a(k_1)a(k_2)\bar{a}(k_3)}{|k_1 k_2 k_3 k|^\sigma} \delta(k_1 + k_2 - k_3 - k)\,\mathrm{d}k_1\,\mathrm{d}k_2\,\mathrm{d}k_3. \tag{11}$$

Note the $-$ $(+)$ sign which labels focusing (defocusing) nonlinearity. This model depends upon two real parameters, $\alpha > 0$ and σ. The parameter σ controls the nonlinearity and the parameter α controls the dispersion relation,

$$\omega(k) = |k|^\alpha. \tag{12}$$

For $\alpha < 1$, this one-dimensional model supports resonant quartets; that is, there exist nontrivial $(k \neq k_1, k_2)$ solutions of the four-wave resonance conditions (6). Note that $\alpha = 2$, $\sigma = 0$ constitute the usual cubic nonlinear Schrödinger equation, with no nontrivial four-wave resonances. The case of $\alpha = \frac{1}{2}$ and $\sigma = -\frac{3}{4}$ mimics dispersion and nonlinear interaction for water waves. But, as stressed above, the wide range of tunable parameters permits systematic studies of various dynamical aspects of dispersive wave turbulence.

Next, to acquire some simple physical intuition and to obtain the kinetic equation of WT for our system, we sketch the closure derivation for $n(k, t)$ (e.g., see [19]), starting with Eq. (11) in k-space, one obtains

$$n_t(k,t) = \pm \int \frac{2\mathrm{Im}\langle a_{k_1} a_{k_2} \bar{a}_{k_3} \bar{a}_k\rangle}{|k_1 k_2 k_3 k|^\sigma} \delta(k_1 + k_2 - k_3 - k)\,\mathrm{d}k_1\,\mathrm{d}k_2\,\mathrm{d}k_3 \tag{13}$$

for the two-point function $n(k, t) = \langle a_k(t)\bar{a}_k(t)\rangle$. Under a Gaussian random phase approximation, and the assumption that

$$\frac{\partial}{\partial t}\langle a_{k_1} a_{k_2} \bar{a}_{k_3} \bar{a}_k\rangle \approx 0, \tag{14}$$

which is consistent with a second-order perturbation analysis when the nonlinearity is assumed to be weak, one obtains the *closure condition*

$$\mathrm{Im}\langle a_{k_1} a_{k_2} \bar{a}_{k_3} \bar{a}_k\rangle = \mp 2\pi \frac{n_2 n_3 n_k + n_1 n_3 n_k - n_1 n_2 n_k - n_1 n_2 n_3}{|k_1 k_2 k_3 k|^\sigma} \delta(\omega_1 + \omega_2 - \omega_3 - \omega). \tag{15}$$

Under this closure condition, Eq. (13) reduces to

$$\dot{n}_k = 4\pi \int \frac{n_1 n_2 n_3 n_k}{|k_1 k_2 k_3 k|^{2\sigma}} \left(\frac{1}{n_k} + \frac{1}{n_3} - \frac{1}{n_2} - \frac{1}{n_1} \right) \delta(\omega_1 + \omega_2 - \omega_3 - \omega) \delta(k_1 + k_2 - k_3 - k)\, \mathrm{d}k_1\, \mathrm{d}k_2\, \mathrm{d}k_3. \quad (16)$$

Eq. (16) is the kinetic equation for $n(k, t)$. Note that Eq. (16) does not depend upon the sign of nonlinearity.

2.2. The wave spectra

Time independent (stable) solutions of the WT kinetic equations (16) describe steady-state spectra:

$$n(k) = c, \text{ equipartition of particle number} \quad (17)$$

$$n(k) = \frac{c}{\omega(k)}, \text{ equipartition of energy} \quad (18)$$

$$n(k) = c|k|^{8\sigma/3-1}, \text{ direct cascade} \quad (19)$$

$$n(k) = c|k|^{8\sigma/3-1+\alpha/3}, \text{ inverse cascade.} \quad (20)$$

The first two "equilibrium spectra" can immediately be shown to satisfy (16). In fact, each is a special case of the general solution,

$$n(k) = \frac{c}{\omega(k) + \mu},$$

where μ is the "chemical potential." Their interpretation as "equipartition of particles" and "equipartition of energy" comes from the invariant

$$\int qq^* \,\mathrm{d}x = \int aa^* \,\mathrm{d}k = \int n(k)\,\mathrm{d}k,$$

and from the "linear energy"

$$\int \omega(k) a(k) a^*(k)\,\mathrm{d}k = \int \omega(k) n(k)\,\mathrm{d}k.$$

Very generally, Zakharov [18] showed that the other two spectra of the "direct" and "inverse" cascades also are steady-state solutions. His argument uses a conformal transformation, and is motivated and described in [9] for our system (10).

In the numerical experiments reported in [3,9], another spectrum (the MMT spectrum) was observed. For Eq. (10) at $\alpha = \frac{1}{2}$, this spectrum is

$$n(k) = c|k|^{2\sigma-(5/4)} \text{ MMT}. \quad (21)$$

The MMT spectrum is not a steady solution of the WT kinetic equation (16) [9]. Rather, it satisfies an alternative closure which was heuristically proposed in [9].

2.3. Summary of earlier results

In our initial work [9] on dispersive wave turbulence, we (i) introduced the model (10); (ii) described numerical experiments, together with their validation and control, in which the MMT spectrum (rather than the direct or inverse cascades of WT theory) was observed and (iii) presented a heuristic closure whose steady solution is the

MMT spectrum. These studies used a pseudospectral numerical method in combination with an integrating factor algorithm, randomly forced (with Gaussian white-noise in time) at the long spatial scales, and damped selectively on both long and short spatial scales with a dissipation of the form (in k-space)

$$-\mathrm{i}[\nu^{-}|k|^{-d} + \nu^{+}|k|^{d}]a_k \tag{22}$$

with the parameter d set to be 8. Here the constants $\nu^{\pm}$ are chosen such that there is a sufficiently wide inertial range in our numerical experiments.

More recent work, reported here and in Refs. [3,5], also used a pseudospectral method in combination with an integrating factor algorithm. For the time dynamics, we used a fourth-order adaptive stepsize Runge–Kutta integrator. (A second-order symplectic time-integrator was also used for numerical verification. No significant differences were observed between these two integrators.) For most of these experiments, the total number of Fourier modes is 2^{13}, and the system size $L \sim 400$.

In recent studies [3,5] we replaced selective dissipation (22) with

$$-\mathrm{i}\Gamma_j a_k, \quad j = \mathrm{l}, \mathrm{s} \tag{23}$$

with Γ_{l} restricted to large spatial scales $|k| \sim 1$, Γ_{s} to small spatial scales $|k| > K_{\mathrm{d}}$ ($K_{\mathrm{d}} = 2600$ for most experiments) and no damping in-between. We also use this constant dissipation (23) in this paper, except in Section 3 on selective dissipation. In [3,5] both deterministic and random (white-noise in time) forcings were studied.

In the numerical experiments reported in [3], four distinct stable spectra were observed — the direct and inverse cascades of WT theory, thermal equilibrium, and a fourth spectrum (MMT). Each spectrum can describe long-time behavior, and transitions between them may occur — depending upon details of nonlinearity, forcing, and dissipation. Cases of a long-lived MMT transient state decaying to a state with WT spectra, and vice versa, were observed.

An important result in [3] is the numerical confirmation of WT spectra for the model equation (10), for both the direct and inverse cascades, as well as thermodynamic equilibrium. Fig. 1 is a typical example of the WT direct cascade, which is observed over more than *four* decades of energy scales, and more than *three* decades of spatial scales. This result constitutes the clearest and most striking numerical observation of WT spectra to date.

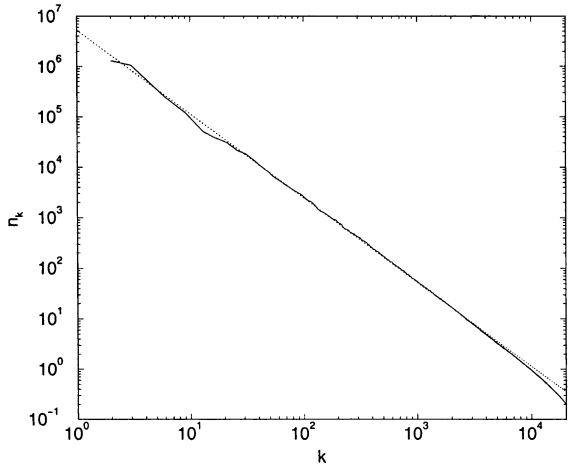

Fig. 1. Direct cascade WT spectrum for a freely decaying dispersive wave (defocusing nonlinearity, $\alpha = \frac{1}{2}$, $\sigma = -0.125$) [3]. The slope of the dotted line is the prediction of the WT theory for direct cascade. The total number of modes here is 2^{16}. Here and throughout this paper, the wavenumber $= 2\pi k/L$, $k \in$ integers.

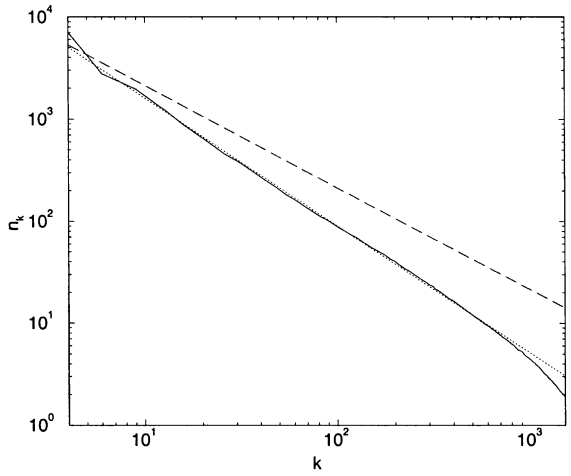

Fig. 2. MMT spectrum of driven-damped dynamics (defocusing nonlinearity with $\alpha = \frac{1}{2}$, $\sigma = 0$). The system is driven by a random force at $2 \leq |k| \leq 3$ and is damped at $|k| = 1$ and $|k| > 2600$. The slope of the dotted line is the prediction of the MMT closure and, for comparison, the dashed line has the slope of the direct WT cascade.

We also verified in [3] the existence of the MMT spectra for both focusing and defocusing nonlinearities. As an example, Fig. 2 shows a case of the MMT spectrum with *defocusing* nonlinearity.

Additional numerical experiments designed to study details of the composition, coexistence, and transition between spectra were briefly described in [3], including: (i) For deterministic forcing, sharp distinctions between focusing and defocusing nonlinearities, including the role of long wavelength instabilities, localized coherent structures, and chaotic behavior; (ii) The role of energy growth in time as a means to monitor the selection of the MMT or WT spectra; (iii) A second manifestation of the MMT spectrum as it describes a self-similar evolution of the

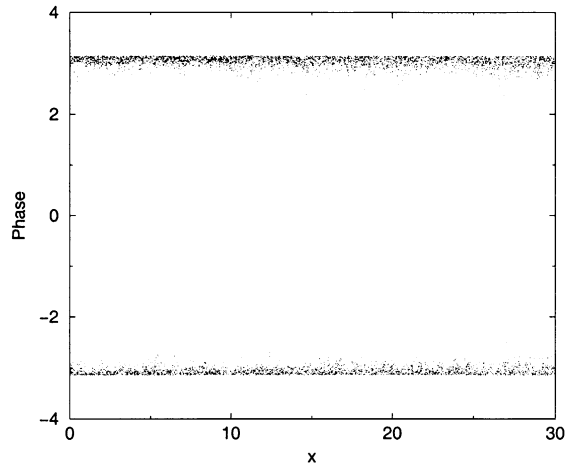

Fig. 3. Phase distribution for the *defocusing* nonlinearity under deterministic drive. In this case, the WT direct cascade is only observed for a very small range of high k's. Plotted is the phase function $\phi(x, t)$ evenly sampled in time, where $\phi(x, t) = \operatorname{Arg} q(x, t)$, of the wave $q(x, t)$. The phase of the wave is nearly "locked" (at $\phi \sim \pi$) to the external forcing, with a small random spattering around the locking phase. (Note that π and $-\pi$ should be identified.).

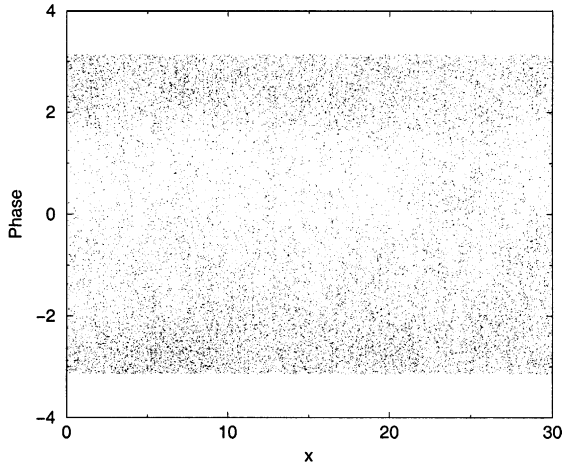

Fig. 4. Chaotic phase distribution for the *focusing* nonlinearity under deterministic drive when the WT direct cascade is observed over almost the entire inertial range. Plotted here is the phase function $\phi(x, t)$ (see Fig. 3).

wave, *without temporal averaging*; (iv) Coherent structures and the evolution of the direct and inverse cascades; (v) Nonlocality (in k-space) of the transferral process.

In [5], properties of the turbulent state are contrasted between focusing and defocusing nonlinearities. The numerical experiments show a clear distinction between the focusing and defocusing cases in the manner and efficiency by which the deterministic force at small k is converted into an "effective random stirring" of the intermediate spatial scales. In the focusing case, this conversion is very efficient, relies on the modulational instability, and involves only modes for relatively small values of k. On the other hand, in the deterministic defocusing case, the absence of the modulational instability forces the conversion to be less efficient, and to take place through a larger range of k modes (presumably through a breakdown of KAM tori). Numerical experiments in [5] with deterministic constant

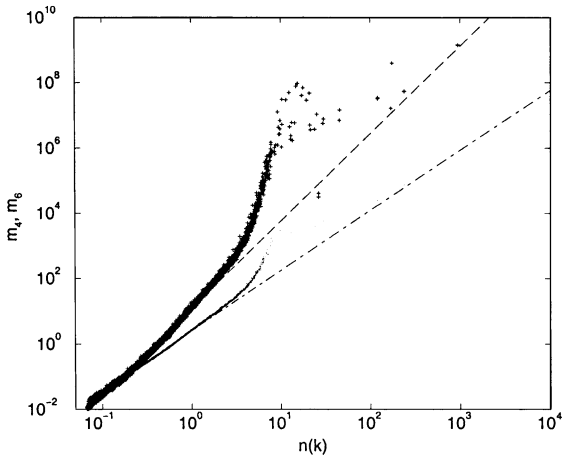

Fig. 5. Deviation from Gaussianity for the *defocusing* nonlinearity under deterministic drive. In this case, the WT direct cascade is only observed for a very small range of high k's. The best fit (dashed line) for the nearly power law tail for the sixth moment (crosses) as a function of second moment is $m_6 = 11.9{m_2}^{2.62}$ and the best fit (dot-dashed line) for the fourth moment (dots) is $m_4 = 2.54{m_2}^{1.84}$. Note that $m_2 = n(k)$ and the relations $m_6 = 6{m_2}^3$ and $m_4 = 2{m_2}^2$ hold for Gaussian distributions.

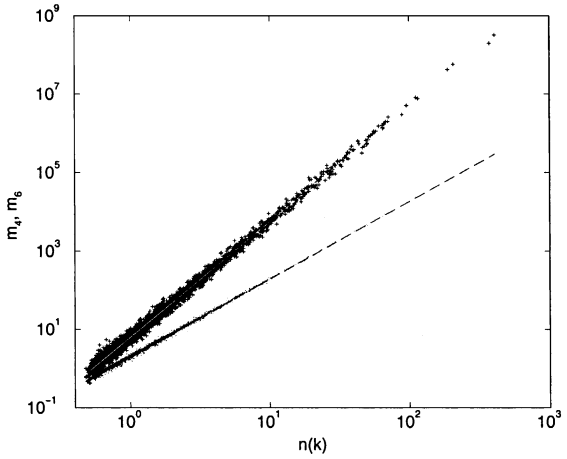

Fig. 6. Gaussianity for the *focusing* nonlinearity under a deterministic drive. In this case, the WT direct cascade is observed over almost the entire inertial range. The best fit for the sixth moment (crosses) as a function of second moment is $m_6 = 6.30{m_2}^{2.95}$ (white line) and for the fourth moment (dots) is $m_4 = 2.05{m_2}^{1.98}$ (dashed line). Note that $m_2 = n(k)$ and the relations $m_6 = 6{m_2}^3$ and $m_4 = 2{m_2}^2$ hold for Gaussian distribution.

forcing also demonstrate that, in the focusing case, the phases of the waves are much more uniformly randomized and the wave amplitudes are much more Gaussian than for the defocusing nonlinearity (see Figs. 3–6), indicating the validity of a WT description of wave turbulence. For the defocusing case, a sufficiently strong nonlinearity is required for a possible chaoticization of wave motions. Note that, however, WT theories are often justified on the ground of weak nonlinearity. This obviously raises an interesting theoretic issue of identifying spatial and temporal scales of decoherence for the onset of WT for the defocusing nonlinearity under deterministic forcing.

Another consequence of the focusing nonlinearity is the formation (through the modulation instability) of spatially localized coherent structures in the wave field, which then interact with the resonant radiation. This interaction is shown in [3,5] to be an essential component of the turbulent cascades and energy transfer cycles in the focusing case for model (10). These turbulent cycles are studied in detail in this article.

3. MMT–WT crossover vs persistence of the MMT spectrum

As mentioned above, for focusing nonlinearity under random driving, a transition takes place from the MMT spectrum to the WT direct cascade. Here, we discuss in detail how the "crossover time scale" from the MMT regime to that of WT is controlled by the driving strength. We also point out that the MMT scaling can arise as a statistically steady front in k-space which separates the WT regime from the dissipation regime.

The MMT–WT crossover: First, we report our numerical results on the MMT–WT crossover of system (10) with focusing nonlinearity, which is driven by a Gaussian white random forcing and damped with the dissipation of the form (23). We describe three numerical experiments, which are initialized with the same smooth initial data, and are driven with three different amplitudes of forcing. (The damping strengths $\Gamma_{\mathrm{l,s}}$ remain fixed for all these cases.) Fig. 7 shows the corresponding temporal growth of the L^2 norm for these experiments. Clearly, it can be seen that, when driving is large, the growth of norm is fast and the total averaged norm is large in the final steady state. With decreasing amplitude of forcing, the norm (and the amplitude of nonlinearity) decrease; hence, the time scale for wave interaction becomes long. Prior to the points labeled by d, g, and i in Fig. 7, the system exhibits a

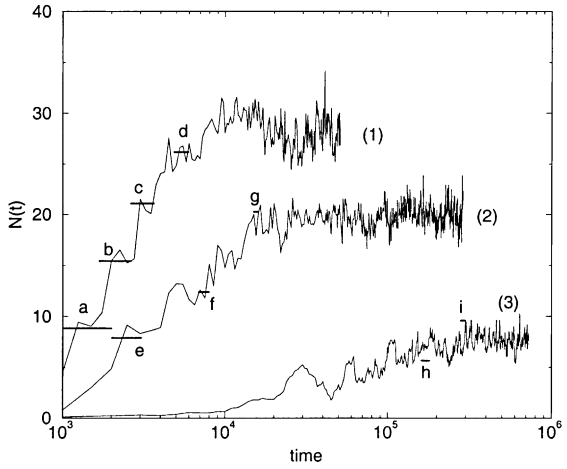

Fig. 7. Temporal growth of L^2 norm $[N(t)]$. a–d correspond to the four spectra in Fig. 8. e–g correspond to the three spectra in Fig. 9. h and i correspond to the two spectra in Fig. 10. The location and the length of the horizontal line segment, indicate the time, and the time window, used in averages to obtain the corresponding spectrum. Case (1) has the largest amplitude of forcing, while case (3) has the weakest amplitude of forcing. Note that time is on a logarithmic scale.

coexistence of the MMT spectrum and WT direct cascade spectrum as shown in Figs. 8–10. We can correlate each stage of expansion of the WT spectrum and contraction of the MMT spectrum with the growth of L^2 norm. For example, the case of strong forcing is shown in Fig. 7 (Curve 1) with four stages labeled by a, b, c, and d. The location and the length of corresponding line segment indicate the time and the time window used in averages to obtain the corresponding spectrum shown in Fig. 8. Similar situations are shown in Figs. 9 and 10 for intermediate and weak forcings, respectively. For times greater than those of the points labeled d, g, and i, the norm fluctuates in time about a constant mean, and the WT direct cascade finally establishes itself as a statistically steady state in all three cases. When the drive becomes weak, the norm grows extremely slowly and the resulting weak nonlinearity

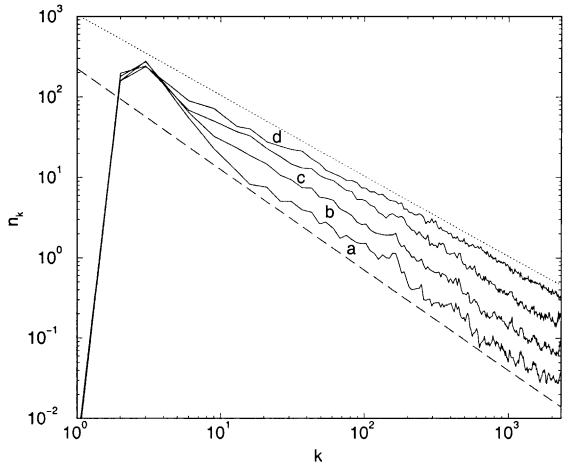

Fig. 8. Transition (a → d) from the MMT regime to the WT direct cascade (focusing nonlinearity with $\alpha = \frac{1}{2}, \sigma = 0$). The system is driven by a random force at $2 \leq |k| \leq 3$ and is damped at $|k| = 1$ and $|k| > 2600$ with $\Gamma_{1,s} = 10$. The slope of the dashed (dotted) line is the prediction of the MMT (WT) closure.

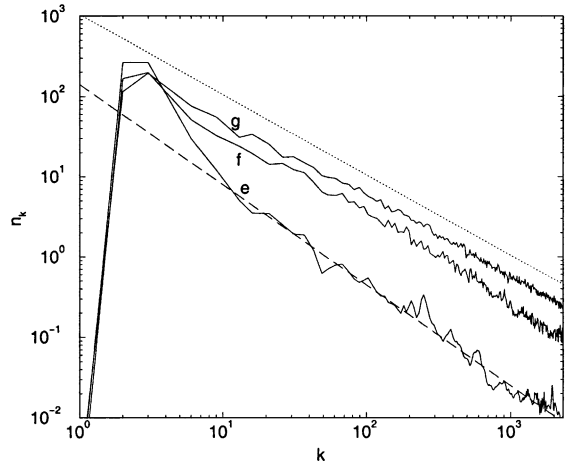

Fig. 9. Transition (e → g) from the MMT regime to the WT direct cascade (focusing nonlinearity with $\alpha = \frac{1}{2}, \sigma = 0$). The system is driven by a random force at $2 \leq |k| \leq 3$ with a weaker strength than that in Fig. 8. There is damping at $|k| = 1$ and $|k| > 2600$, with the same damping strength as the case shown in Fig. 8. The slope of the dashed (dotted) line is the prediction of the MMT (WT) closure.

leads to a very large time scale for the crossover as shown in Fig. 7 (Curve 3) (note that the time scale in Fig. 7 is logarithmic). From case (2) to (3) in Fig. 7, the total norm is reduced (approximately) by a factor of 2, while the MMT–WT turn-over time in case (3) (i.e., the time at point i) is more than 10 times longer than that in case (2) (the time at the point labeled by g). In this weakly nonlinear regime, our results show that the MMT spectrum can live for a *very* long time — precisely in the regime in which WT theory is supposed to be valid. In this regime, the nonlinear turnover time scale can be very long because the nonlinearity is very weak; therefore, an important theoretic issue is to delimit the temporal validity of the spectra of dispersive wave turbulence. In the next paragraph,

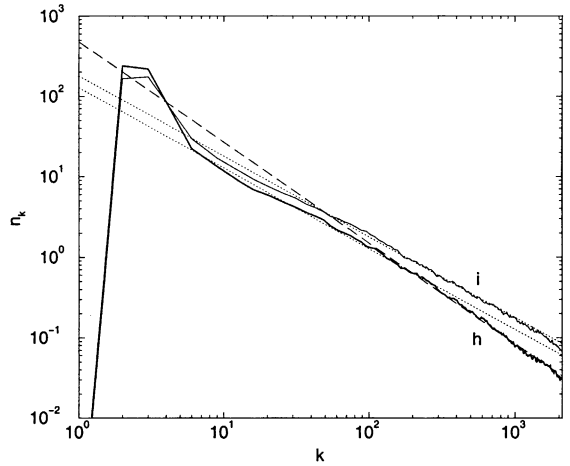

Fig. 10. Transition (h → i) from the MMT regime to the WT direct cascade (focusing nonlinearity with $\alpha = \frac{1}{2}, \sigma = 0$). The system is driven by a random force at $2 \leq |k| \leq 3$ with a weaker strength than that in Fig. 9. There is damping at $|k| = 1$ and $|k| > 2600$ with the same damping strength as the case shown in Fig. 8. The slope of the dashed (dotted) line is the prediction of the MMT (WT) closure.

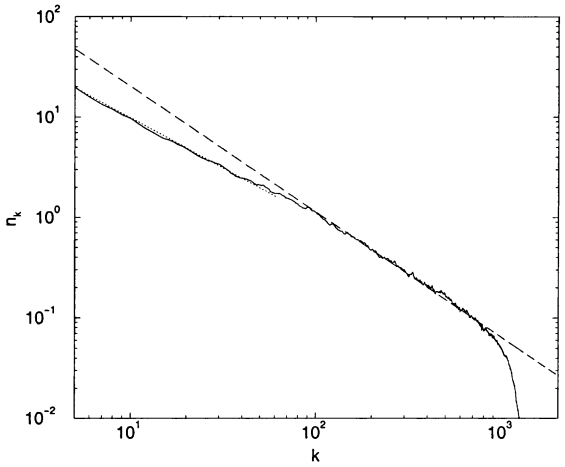

Fig. 11. Persistence of the front described by the MMT spectrum, which separates the WT direct cascade and the dissipation range (focusing nonlinearity with $\alpha = \frac{1}{2}$ and $\sigma = 0$). The damping used here has the form described by Eq. (24) with $K_\mathrm{d} = 1000$, $p = 4$. The slope of the dashed (dotted) line is the prediction of the MMT (WT) closure.

we show that the MMT spectrum can actually persist as a stable front in k-space which separates the WT spectrum from the dissipation range — in a very weak nonlinear regime, induced by strong damping.

Persistence of the MMT spectrum: Here, we consider a very weak nonlinear regime as signified by small total norms (e.g., usually below the steady part of Curve 3 in Fig. 7), with a *strong* dissipation at high k's. The strong dissipation can be achieved with large Γ_s in Eq. (23) or by a "selective dissipation" of the form,

$$-\mathrm{i}\Gamma_\mathrm{s}(k - K_\mathrm{d})^p a_k, \tag{24}$$

where K_d is a dissipation cutoff below which there is no damping. Strikingly, Fig. 11 shows that, in this regime, the MMT spectrum is observed as a *stable* statistically steady matching front between the weak-turbulent direct

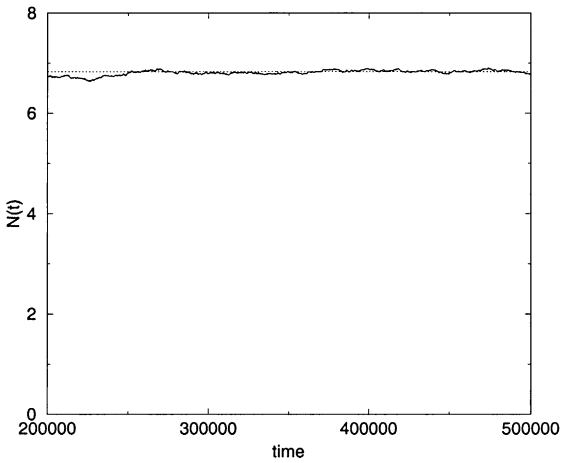

Fig. 12. Fluctuation of norm about a constant (dotted line) for the case of Fig. 11 with a steady MMT regime between the WT direct cascade and the dissipation regime.

cascade and the dissipation range. Unlike the previous case of the MMT–WT crossover, where over the times of constant norm, the MMT spectrum disappears, here, the MMT spectrum persists even when the total norm has reached a statistically steady state. Fig. 12 clearly illustrates this point, in which the norm as a function of time for the statistically steady state of Fig. 11 is shown. We emphasize that this statistically steady MMT matching front is robust for various damping forms, such as Eq. (24) with $p = 4$ or $p = 6$, or the constant damping as in Eq. (23) with a sufficiently large Γ_s. And this statistically steady MMT front occurs regardless of the sign of nonlinearity. Therefore, in addition to the delineation of time scales over which the MMT and WT spectra can be observed, there is also the issue of delineating spatial scales over which the MMT and/or WT spectra can persist. Here, we have clearly demonstrated that there are regimes in which the WT direct cascade at intermediate spatial scales can coexist with a stable MMT spectrum at shorter spatial scales.

4. Energy transfer cycles and cascades

Traditionally, WT theory primarily concerns the weakly nonlinear limit, where only wave–wave resonant interactions control energy transfer in k-space — as signified in the kinetic equation (16), which involves only resonant quartets of waves and does not discriminate the sign of nonlinearity. However, the original system (10) can display quite different dynamics, depending upon which sign of nonlinearity is chosen. For the defocusing nonlinearity, the system has a definite Hamiltonian, with linear-like waves. Whereas, for the focusing nonlinearity, the system has an indefinite Hamiltonian and its long waves may be subject to modulational instability, thus inducing coherent solitonic excitations, which may in turn lead to waves which collapse in space in finite time. When there is a generation of coherent excitations in the system, it can be argued that the applicability of WT theory to this regime may be questioned since the nonlinearity is no longer small. However, there is a dynamic regime in which the nonlinear term remains small for *short* waves, while simultaneously *long* waves form nonlinear coherent excitations through the modulational instability. It can be expected that the statistical behavior of these spatially localized coherent structures can be captured by a "most probable state description" which predicts these states live in thermodynamic equilibrium [4,8]. In this section, we address the following issue: what roles do these coherent excitations, together with resonant quartets, play in energy transfer within this regime of moderate nonlinearity — where, the nonlinear terms become significant for the long waves. (In contrast, we note in passing that for the defocusing case, at moderate nonlinearity, it can be expected that the dynamics of high k waves can be described by a cascade of renormalized near-linear waves, which are weakly interacting.)

In this section, for the focusing case, we present a detailed numerical study of energy transfer throughout the entire range of spatial scales — a cycle of energy transfer for dispersive wave turbulence which involves the interaction of coherent structures and resonant waves as they form the equilibrium, inverse and direct WT cascades simultaneously. First, we describe the formation of two distinct types of coherent structures for the forced and free cases, and their associated energy transport from small k to large k. Then, we precisely characterize turbulent cycles for strongly driven, moderately driven, and freely decaying turbulence.

4.1. Formation of coherent structures

As described above, the modulational instability in focusing dynamics induces spatially coherent "solitonic" excitations at random spatial locations to form a thermal equilibrium state (Fig. 13). The energy injection process associated with the creation of these localized excitations is a fast process, while the decay of these coherent structures is slow. There are two extreme cases for the formation of the localized excitations: (i) the self-similar collapse in a *free* wave system and (ii) a focusing event for *driven-damped* wave.

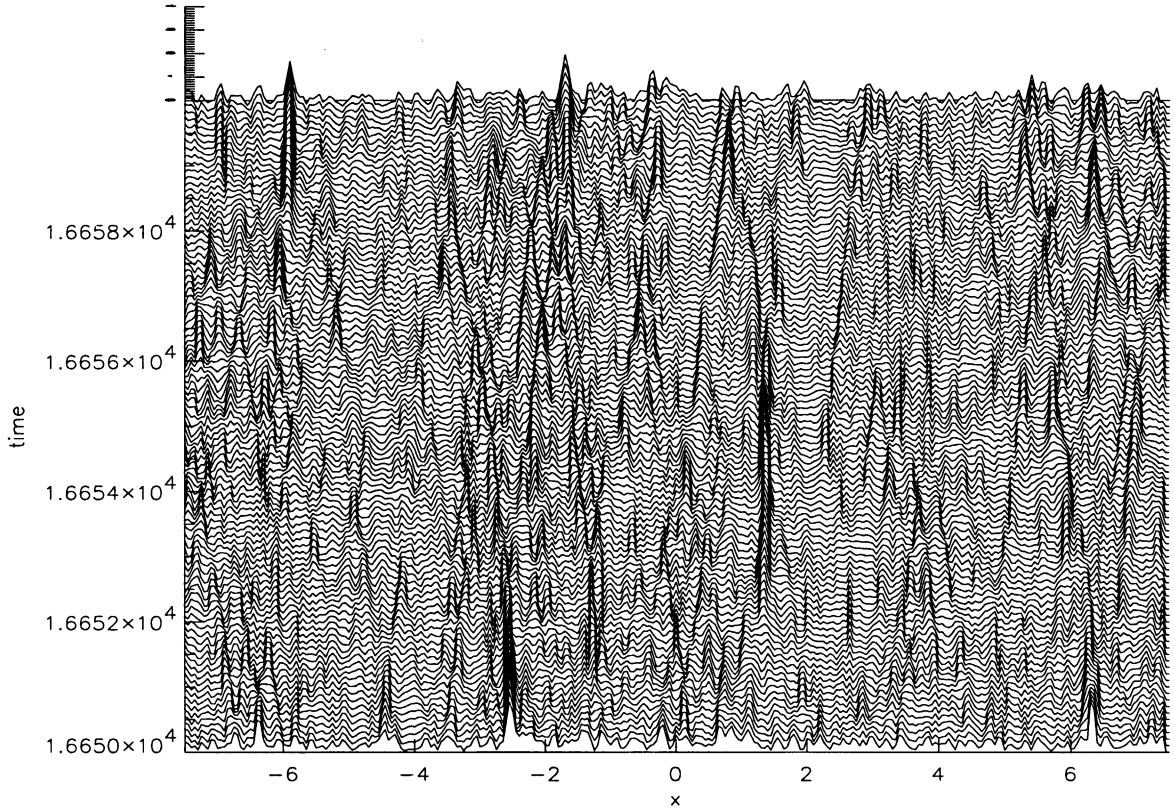

Fig. 13. Formation of the coherent structures, their saturation, and the generation of the inverse cascades (which can be observed in the decay process of localized structures into long wavelength radiation). Plotted here is the space–time profile of $|q(x,t)|$ ($\alpha=\frac{1}{2}$, $\sigma = 0$, focusing nonlinearity).

Free wave case: Fig. 14 illustrates this fast process of energy injection of the collapse, in which an isolated solitonic structure in the initial data becomes a highly focusing, self-similar event, transferring energy into small scales. We note that the free wave equation (11) admits self-similar collapsing solutions of the form,

$$a_k = \tau^{-((4\sigma+\alpha-2)/2\alpha)} R(\eta) \exp(\mathrm{i}\theta \log \tau), \tag{25}$$

where $\tau = |t - t_0|$, $\eta = k\tau^{1/\alpha}$ and $\sigma < \frac{1}{4}(1-\alpha)$ (t_0 is the collapse time). One can show analytically that, for this collapse, the wave front propagation in k-space of the instantaneous $n(k,t) = a(k,t)\bar{a}(k,t)$ possesses an envelope function $S(k)$ of the following scaling:

$$S(k) \sim k^{4\sigma+\alpha-2}. \tag{26}$$

Incidentally, we note that this exponent is related to the Phillips spectrum for water waves [12,13], and (at $\sigma = -\frac{3}{4}$) is exactly the spectrum studied in [20] for the model (10).

For the collapsing wave shown in Fig. 14, the associated wave front propagation in k-space is shown in Fig. 15. It can be clearly seen that the exponent of the envelope is well described by Eq. (26).

Driven-damped wave: With sufficiently strong driving and damping, the second kind of focusing waves occurs — one which possesses the MMT exponent for the envelope of its propagating wave fronts in k-space. This is

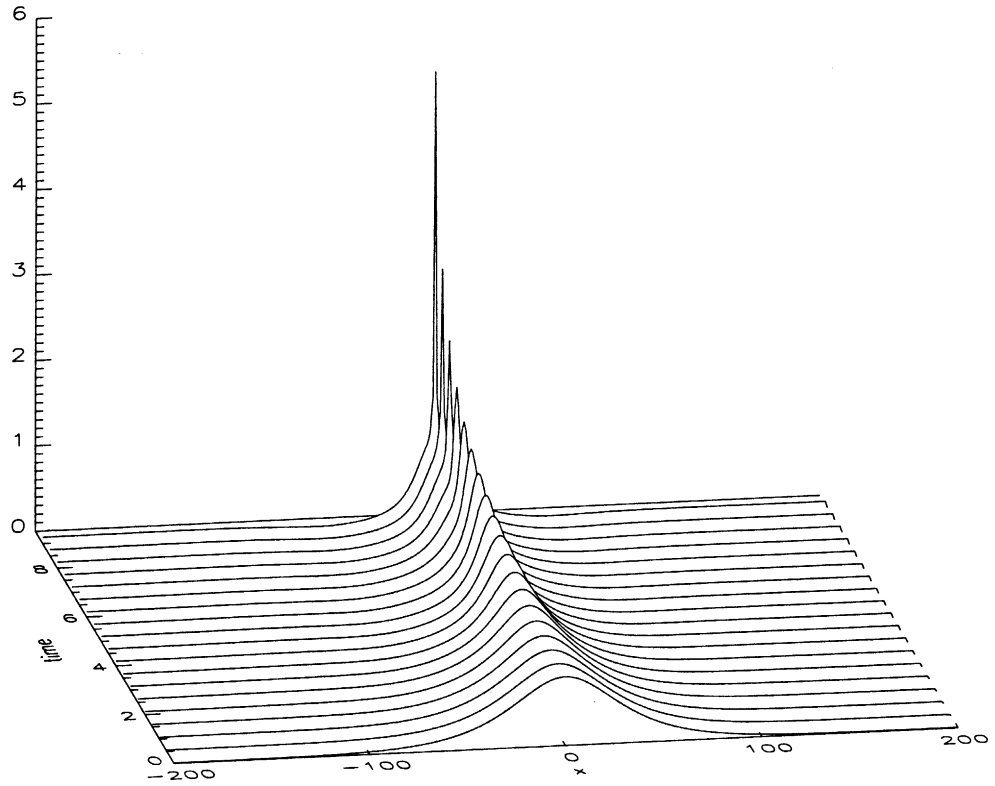

Fig. 14. Fast injection of energy into small scales for the focusing nonlinearity: an initially localized coherent structure evolves into a highly focused event, $\sigma = 0$, $\alpha = \frac{1}{2}$. The initial data is of the form $A\,\mathrm{sech}(bx)$, where A and b are constants.

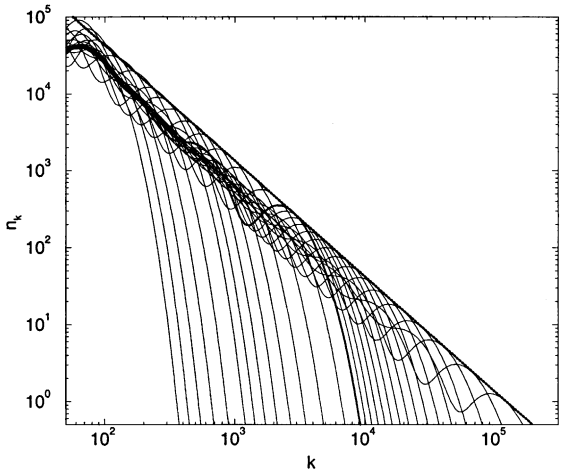

Fig. 15. Collapsing wave front in k-space: *solutions* for the *focusing* nonlinearity ($\alpha = \frac{1}{2}$, $\sigma = 0$) for the *free wave* evolving from a smooth initial data. Note that *no time average* is used here. Each curve represents $n(k,t) = a(k,t)\bar{a}(k,t)$ at a different time. (The solutions after the thick curve are advanced in an even time interval, others are not necessarily evenly sampled in time.) The large k envelope exhibits the collapse exponent (Eq. (26)) (dotted line). The total number of modes here is 2^{19}.

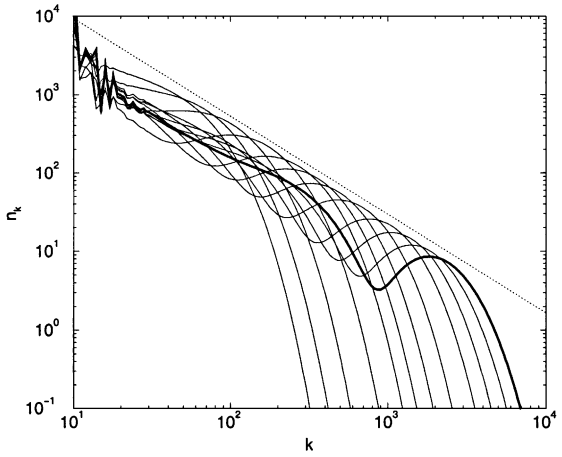

Fig. 16. Wave motion in k-space: *solutions* for the *focusing* nonlinearity ($\alpha = \frac{1}{2}, \sigma = 0$), *driven by a steady force* on $1 \leq |k| \leq 2$ and damped on $|k| = 1$, evolving from a smooth initial data. Note that *no time average* is used here. Each curve represents $n(k, t) = a(k, t)\bar{a}(k, t)$ at a different time (not necessarily evenly sampled). The large k envelope exhibits the MMT exponent (dotted line).

demonstrated in Fig. 16, in which the envelope of $n(k, t) = a(k, t)\bar{a}(k, t)$, evolving from a smooth initial data (*without time average*) exhibits the MMT exponent.

4.2. Energy transfer cycles

The formation of spatially localized excitations can actively transfer energy into high k_s via their focusing processes in space, where the order of magnitude of wavenumber k_s is determined by the spatial scale at which these localized waves saturate. When the forcing is strong, hence strong nonlinearity, the propagation of the wave front in k-space saturates at short scales within the dissipation range. One anticipates that, once it reaches the dissipation scale, the localized structure starts to decay via emission of long-wave radiation. Fig. 17 confirms this scenario, in which the focusing event in Fig. 14 slowly decays by emitting radiation of various long wavelengths, gradually transferring the energy back from small scales to large scales via resonant quartets. Clearly, this energy transfer process should initiate an inverse cascade.

At large forcing amplitudes, the saturation process occurs at very short wavelengths, and k_s resides within the dissipation range; however, at moderate forcing amplitudes, the saturation process occurs at intermediate spatial scales, and k_s can reside in the middle of the inertial range. In the former case, as shown in Fig. 17, some radiation is dissipated and some generates, through resonant quartet interactions, an inverse cascade toward long wavelengths — where the modulational instability acts to create self-focusing coherent structures and to complete the cycle. In the latter case (of moderate forcing amplitudes), the localized structures saturate in the center of the inertial range, where they generate, again through resonant quartet interactions, both the direct (toward shorter scales) and the inverse (toward longer scales) cascades. Dissipation terminates the flux toward shorter scales, and the modulational instability terminates the flux (of the inverse cascade) toward longer scales. And again, the process cycles. Fig. 18 illustrates schematically the energy transfer cycle in these two situations.

Cycles in driven-damped case: Our numerical spectra, such as for the case depicted in Fig. 13, confirms these cycles of energy transfer. Fig. 19(a) provides an excellent example of the coexistence of a thermodynamical equilibrium of coherent structures with the inverse cascade induced by their slow generation of long wave radiation. For spectrum

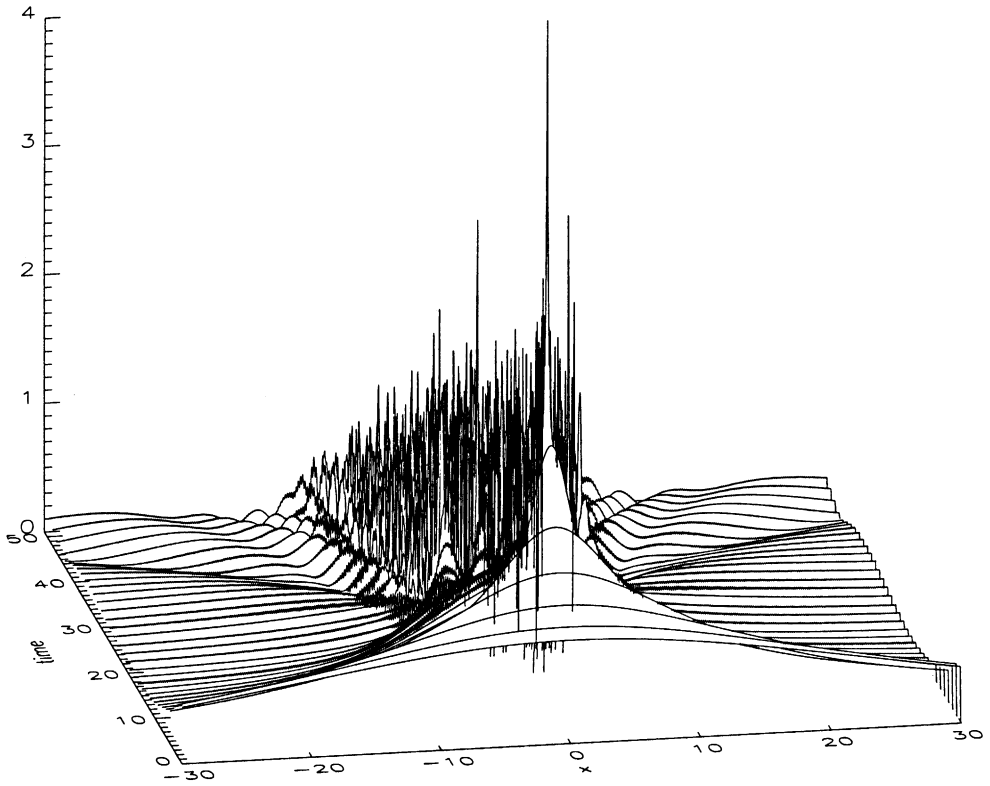

Fig. 17. Decay of a coherent structure initiates inverse cascade of energy by transferring energy from small scales to large scales via radiation.

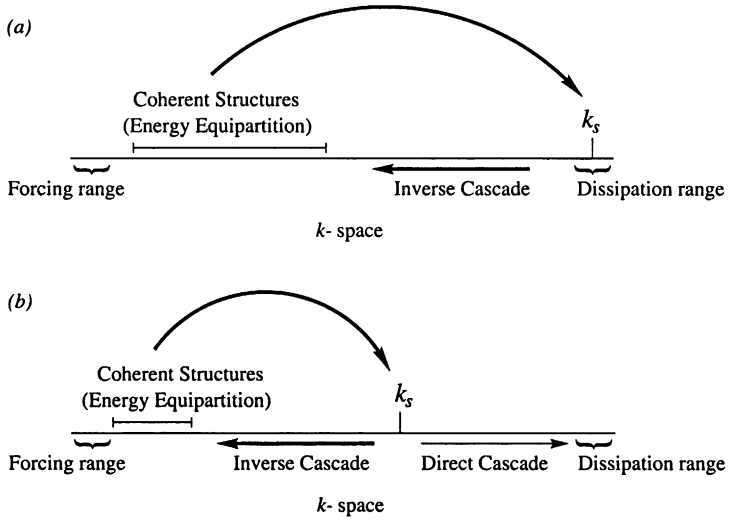

Fig. 18. The cycle of energy transfer in dispersive wave turbulence: (a) The saturation scale k_s of the spatially localized coherent structures is in the dissipation range — coexistence of energy equipartition and the WT inverse cascade; (b) The saturation scale k_s of the spatially localized coherent structures is in the middle of the inertial range — coexistence of the WT inverse cascade and direct cascade.

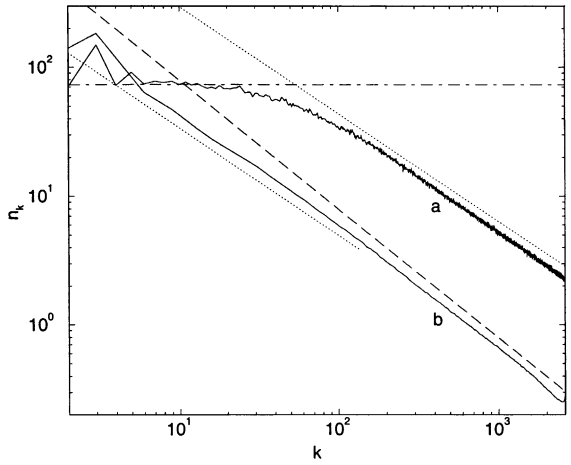

Fig. 19. (a) Coexistence of thermodynamical equilibrium and the *inverse* WT cascade, for the *focusing* nonlinearity ($\alpha = \frac{1}{2}, \sigma = 0$), driven by a steady force on $|k| = 1$. The flat part of the spectrum (dot-dashed line) shows thermodynamical equilibrium. (b) Coexistence of the *inverse* and *direct* WT cascades. The dotted (dashed) line has the exponent of inverse (direct) WT cascade.

(a), we have $k_s > 1000$. We note that, for k greater than k_s, the usual WT direct cascade should be expected, since the coherent excitations do not have strong influence on energy transfer at spatial scales much smaller than their coherence length. Fig. 19(b) demonstrates this phenomenon, where, by reducing forcing, we have tuned to a regime such that only very few long waves are unstable. These inject energy into $k_s \sim 100$, resulting in an inverse cascade for $k < k_s$ and a direct cascade for $k > k_s$. Incidentally, the quantity, $R \equiv |(H_0 - H)/H|$, can be used to indicate the strength of nonlinearity, where H_0 is the total kinetic (linear) energy (Eq. (9)) and H is the total energy (Eq. (7)). For spectrum (a), $R \sim 20\%$, indicating relatively strong nonlinearity (especially, for long waves as we discussed above). However for spectrum (b), $R < 3\%$, signifying weak nonlinearity over the entire inertial range.

Cycles in freely decaying case: In a freely decaying situation, the cycle changes dynamically. The results are captured in Fig. 20, in which we use the final state of the numerical experiment depicted in Fig. 19(a) as the initial state, which then freely decays without any forcing. As the turbulence decays, the saturation scale k_s moves from the high-k dissipation scale of strong nonlinearity, where it exhibits a strong inverse cascade originated near the dissipation scale (Fig. 20(b)); then it moves through the intermediate inertial range where both cascades appear (Fig. 20(c)); finally moving to the low-k injection range, where only a WT direct cascade remains (Fig. 20(d)). This latter state is very much linear-wave like, as shown in Fig. 21 (best viewed with an oblique angle with the paper). This near linear state is in sharp contrast to the violent wave motions associated with the formation of coherent structures as captured in Fig. 13.

Fig. 22 illustrates schematically this temporal dynamics of energy cycles with decreasing k_s. The decay of the associated L^2 norm is shown in Fig. 23, in which the thick segments indicate the time average window used for obtaining the corresponding spectra in Fig. 20. The cycle of energy transfer in the freely decaying setting shows that the mechanism determining the saturation scale is due to the strength of nonlinearity (which is controlled by the amplitude of forcing in the damp-driven situation).

Finally, we emphasize that *defocusing* dynamics does not possess this energy transfer cycle, even when driven extremely strongly, e.g., a value so strong that the total norm is increased by a factor of 10^2 with respect to the cases shown in Fig. 19. This is simply because the defocusing nonlinearity does not have long wave instabilities and *localized* excitations.

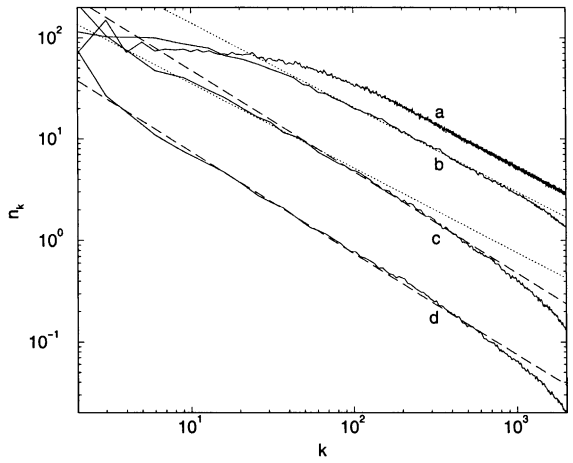

Fig. 20. Cycle of energy transfer in a *freely decaying* dispersive wave ($\alpha = \frac{1}{2}, \sigma = 0, |K_d| = 2600$ and focusing nonlinearity). (a) The spectrum associated with the initial state of the decay process; (b) An inverse cascade of WT originating near the dissipation scale; (c) Coexistence of inverse and direct cascades when the saturation scale k_s is in the intermediate inertial range; (d) A WT direct cascade remains when the saturation scale k_s decreases to the low-k injection range. The dotted line has the exponent of the WT inverse cascade and the dashed line has that of the WT direct cascade.

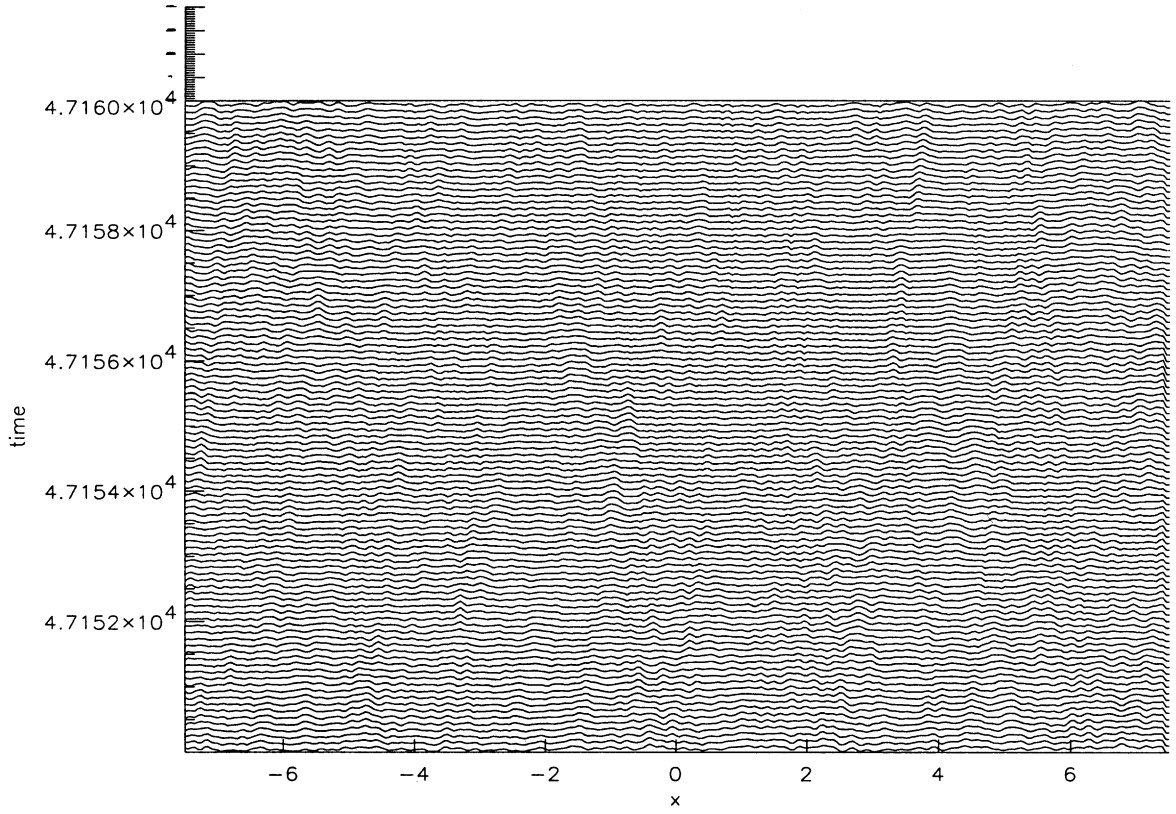

Fig. 21. Spatio-temporal evolution for which only direct WT cascade is observed in a freely decaying wave turbulence. Plotted here is the space–time profile of $|q(x,t)|$. The scales of x, t and $|q|$ are the same as those in Fig. 13 ($\alpha = \frac{1}{2}, \sigma = 0$, focusing nonlinearity).

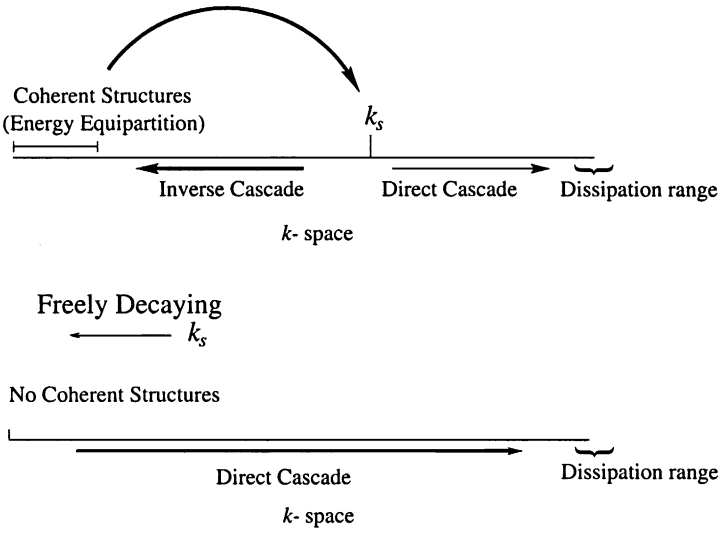

Fig. 22. The cycle of energy transfer for a freely decaying dispersive wave turbulence. The saturation scale k_s decreases as the nonlinearity decreases.

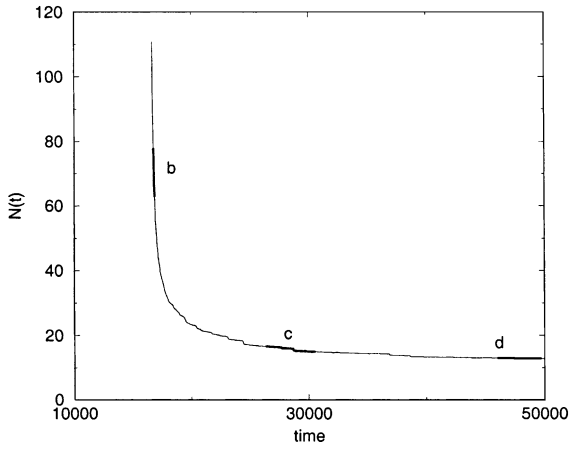

Fig. 23. Temporal decay of L^2 norm. b–d correspond to the three spectra shown in Fig. 20. The location and the time interval of the thick line segment indicate the time and time window used in averages to obtain the corresponding spectrum in Fig. 20.

5. Discussion and conclusion

Taken together, our numerical studies of the one-dimensional model equation (10) (reported here and in [3,5,9]), have established the richness of spectra for dispersive wave turbulence — the direct and inverse cascades of WT theory, thermodynamic equilibrium, and the MMT spectrum. For this model (10), the MMT spectrum often appears in regimes of relatively strong forcing, and has only been observed in driven-damped situations — in sharp contrast to the WT spectra which we have shown appear in the freely decaying case. In fact, our numerical experiments on freely decaying turbulence constitute the most striking confirmation to date of WT theory. The MMT spectrum can be transient in some forcing and damping regimes, and can be persistent in others; it can describe wave front

propagation in k-space of focusing waves, or a statistically steady front which separates the WT cascades and the dissipation range. We emphasize that the MMT spectrum is observed for both defocusing and focusing nonlinearities. The WT spectra of WT theory seem to be intrinsic properties of free waves, whose description is universal in the sense that it does not depend upon the detailed processes of energy injection and dissipation. However, we have demonstrated that, in realistic settings in the presence of forcing and damping, these universal WT spectra may not be observed or may coexist with other spectra. Thus, a comprehensive understanding of dispersive wave turbulence requires the incorporation of effects of forcing and damping on the entire inertial range. Our numerical experiments establish that caution is required when WT theory is applied to practical situations which include forcing and damping — such as in the parametrization of small scales for large scale simulations, or in the theoretical interpretation of wave spectra observed experimentally.

In this article, we have described new numerical results about (i) the coexistence and competition between distinct spectra, throughout spatial and temporal scales; (ii) the role of forcing and damping in the outcome of these competitions and (iii) the interactions between localized coherent structures and resonant radiation in the transport of energy within turbulent cycles. These new results further emphasize that a complete theory of dispersive wave turbulence will require uniform asymptotics in both space and time. This uniformity, together with an effective description of the interaction of localized coherent structures with resonant waves, presents a significant theoretical challenge.

As for the turbulent cycles, we comment that a similar scenario has been argued for optical and plasma turbulence — in which long wave instabilities give rise to collapsing filaments, directly transporting excitations to the high k dissipation regime, leading to cycles of intermittency [6,11]. Clearly, our study of turbulence cycles in model (10) presents a precise and detailed characterization of the role of spatially localized coherent structures as controlling mechanisms in setting up the WT direct and inverse cascades, which in turn give rise to energy transfer cycles across the entire inertial range. In particular, as we have demonstrated above, the energy injection scale, controlled by the strength of nonlinearity, can reside well within the inertial range (not restricted to the high k dissipation range as in [6,11]), thus, leading to fascinating temporal and spatial dynamics of spectra, such as the coexistence of multiple WT spectra in the driven-damped or freely decaying cases. Evidently, this explicit numerical realization of turbulent cycles arises as one of the consequences of the rich mathematical structure possessed by our model (10), in combination with numerical advantages derived from its one-dimensionality.

We note that the intuition about dispersive wave turbulence acquired from our studies of Eq. (10) is not restricted to this idealized class of one-dimensional models. We believe that our numerical study has broad implications about the nature of far more complicated, realistic physical wave turbulence. For example, it is instructive to compare the spectra in Fig. 20 in our freely decaying turbulence with the experimentally observed spectra for a freely decaying turbulence in a thin soap film — which also exhibits the decay of a state described by the coexistence of the direct enstrophy and inverse energy cascades, to a state with only the direct enstrophy cascade [7,14] — where the energy injection scale is controlled by small vortices created upstream. In addition, it is tempting to speculate that the MMT spectrum, associated with the fast injection of excitations by spatially localized coherent structures in our model (10) for the focusing case, may be analogous to the k^{-4} spectrum, which is presumably related to vorticity shocks [15], and which is observed experimentally [7] for "soap film turbulence", in the region near the initial injection, and numerically, in the onset of the coherent eddy formation before the dissipative scales are excited [2].

Furthermore, we observe that, over the years, numerical studies of the spectra of turbulent phenomena have proven difficult, contradictory, and inconclusive. In most of the numerical studies of turbulence, computational limitations severely restrict the decades over which spectra can be observed, making such numerical observations difficult to interpret and to rely upon. As an example of the difficulties in two-dimensional fluid turbulence, different groups [1,16,17] in careful studies observe different and distinct spectra in their numerical experiments. Similar studies of turbulence for fluids with rotation, which are relevant for atmospheric flows, were reported in [10]. In each of these studies, the presence of coherent vortices alters the observed spectra. These distinct observations are very reminiscent

of our observations for model (10) with focusing nonlinearity. In our studies, the distinct time scales associated with different coherent excitations (and the comparison of these time scales with natural mixing and turnover times) produces an interpretation of the mechanisms responsible for the different spectra — an interpretation which is likely to extend to more realistic settings of fluid turbulence. Our numerical studies demonstrate that the one-dimensional class of models introduced in [9] permits precise numerical characterization of rich dynamics of wave turbulence, toward the resolution of issues necessarily left ambiguous in the simulations of more realistic models of turbulence in two and three spatial dimension.

Acknowledgements

David Cai is supported in part by the Joseph and Hebert Keller Instructorship at New York University, and in part by a Sloan Foundation Grant #96-3-1; A.J. Majda is supported by NSF DMS 9972865, DMS 9625795, ONR N00014-96-0043, and ARO-DAAG55-98-1-0129; David McLaughlin is supported in part by a Sloan Foundation Grant # 96-3-1, AFOSR-49620-98, and NSF DSM-9971813; E.G. Tabak is supported by NSF DMS 9701751.

References

[1] V. Borue, Inverse energy cascade in stationary two-dimensional homogeneous turbulence, Phys. Rev. Lett. 72 (1993) 1475–1478.
[2] M.E. Brachet, M. Meneguzzi, H. Politano, P.L. Sulem, The dynamics of freely decaying two-dimensional turbulence, J. Fluid Mech. 194 (1988) 3333–3349.
[3] D. Cai, A.J. Majda, D.W. McLaughlin, E.G. Tabak, Spectral bifurcations in dispersive wave turbulence, Proc. Nat. Acad. Sci. 96 (1999) 14216–14221.
[4] D. Cai, D.W. McLaughlin, J. Shatah, Spatiotemporal chaos and effective stochastic dynamics for a near integrable nonlinear system, Phys. Lett. A 253 (1999) 280–286.
[5] D. Cai, D.W. McLaughlin, Chaotic and turbulent behavior of unstable 1-d nonlinear dispersive waves, J. Math. Phys. 41 (2000) 4125–4153.
[6] S. Dyachenko, A.C. Newell, A. Pushkarev, V.E. Zakharov, Optical turbulence: weak turbulence, condensates and collapsing filaments in the nonlinear Schrödinger equation, Physica D 57 (1992) 96–160.
[7] M. Gharib, P. Derango, A liquid film (soap film) tunnel to study two-dimensional laminar and turbulent shear flows, Physica D 37 (1989) 406–416.
[8] R. Jordan, B. Turkington, C. Zirbel, A mean field statistical theory for the NLS equation, Physica D 137 (2000) 353–378.
[9] A. Majda, D.W. McLaughlin, E.G. Tabak, A one dimensional model for dispersive wave turbulence, J. Nonlinear Sci. 7 (1997) 9–44.
[10] M. Maltrud, G. Vallis, Energy spectra and coherent structures in forced two-dimensional and beta-plane turbulence, J. Fluid Mech. 228 (1993) 321–342.
[11] A.C. Newell, V.E. Zakharov. Optical turbulence, in: P. Tabeling, O. Cardoso (Eds.), Turbulence: A Tentative Dictionary, Plenum Press, New York, 1995, pp. 59–66.
[12] O.M. Phillips, The Dynamics of the Upper Ocean, Cambridge University Press, Cambridge, 1977.
[13] O.M. Phillips, Spectral statistical properties of the equilibrium range in wind-generated gravity waves, J. Fluid Mech. 156 (1985) 505–531.
[14] M.A. Rutgers, Forced 2d turbulence: experimental evidence of simultaneous inverse energy forward enstrophy cascades, Phys. Rev. Lett. 81 (1998) 2244–2247.
[15] P.G. Saffman, On the spectrum and decay of random two-dimensional vorticity distributions of large Reynolds number, Stud. Appl. Math. 50 (1971) 377–383.
[16] L. Smith, V. Yakhot, Bose condensation and small-scale structure generation in a random force driven 2d turbulence, Phys. Rev. Lett. 71 (1993) 352–355.
[17] L. Smith, V. Yakhot, Finite-size effects in forced two-dimensional turbulence, J. Fluid Mech. 274 (1994) 115–138.
[18] V.E. Zakharov, Kolmogorov spectra in weak turbulence problems, Handbook of Plasma Physics, Vol. 2, North-Holland, Amsterdam, 1984, pp. 1–36.
[19] V.E. Zakharov, V. Lvov, C. Falkovich, Kolmogorov Spectra of Turbulence I, Springer, New York, 1992.
[20] V.E. Zakharov, P. Guyenne, A.N. Pushkarev, F. Dias, Wave turbulence in one-dimensional models, 152–153 (2001) 573–619.